Results in Physics 43 (2022) 106110

Contents lists available at ScienceDirect

Results in Physics

journal homepage: www.elsevier.com/locate/rinp

Charge transport in semi insulating bulk 4H-Silicon carbide: Effect of metallization and wafer homogeneity

P. Praus *, M. Betušiak, E. Belas, J. Kunc, R. Grill, M. Brynza, J. Pipek

Charles University, Faculty of Mathematics and Physics, Institute of Physics, Ke Karlovu 5, Prague, Czech Republic

ARTICLE INFO

Keywords:
4H-SiC
Time of Flight
Alpha spectroscopy
Metallization
Polarization effect

ABSTRACT

We investigated the effect of metallization and spatial homogeneity on the charge collection of sensors prepared from high purity semi-insulating 4H-SiC bulk wafer. We used Au, Ni, Cr or graphene electrical contacts subsequently prepared on the same chip. We also tested sensors prepared from different positions on the wafer. Laser-induced transient current technique (L-TCT) and alpha spectroscopy were used to characterize the charge transport in the sensors. It was found that different sensors polarize at DC bias in the time interval of 0.2–270 s. We observed significant deviation of current transients measured on the sensor with a graphene contact from the sensors with metal contacts, which is attributed to the surface plasmon formed on the graphene-SiC interface. We demonstrated that the sensor polarization is independent of the metallization, whereas it strongly depends on the location on the wafer from which the sensor was cut. This testifies to a significant spatial inhomogeneity of the wafer. We also tested the electrical current relaxation after step-DC biasing as a simple method for the characterization of the sensor polarization. We found that the relaxation profile has extremes in the similar positions as the L-TCT profiles of collected charge. We also showed that using pulse biased L-TCT we are able to choose suitable sensors with slow polarization and to design optimal pulsing conditions including necessary depolarization times for the alpha spectroscopy measurement and L-TCT techniques to achieve long-term stable charge collection. In case of ^{241}Am alpha spectroscopy charge collection efficiency 5–24 % was observed. We framed up model depicting all observed phenomena assuming the space charge formation induced by a blocking cathode in an *n*-type material and related lifetime reduction. We evaluated the space charge formed in the sensors after 10^4 s biasing, which ranged from 1.7×10^{14} cm^{-3} to 7×10^{14} cm^{-3} in respective sensors.

Introduction

Wide band–gap silicon carbide (SiC) is usually used for the production of electronic components operating in extremely harsh environments such as in space, and in the automotive, aeronautic and nuclear industries. SiC is currently being explored as an alternative to high-temperature silicon (Si) to overcome the temperature and radiation limitations of commercial Si. SiC has over Si the twofold thermal conductivity, eightfold maximum breakdown electric field intensity, high maximum current density and favourable radiation hardness [1–4]. These properties predetermine SiC to be promising in the thermally stable high–power semiconductor applications and for the production of radiation detectors in which much higher bias can be applied, resulting in higher carrier drift velocities and high charge collection efficiency.

One of the key problems of the wider production of the high performance SiC radiation detectors is the lack of the high-quality large-volume epitaxial layers or bulk single crystals with a low concentration of structural defects and impurities. After the bias application these defects cause the lifetime shortening of photo-generated carriers, low charge collection efficiency and gradual warping of the internal electric field, called detector polarization. Carbon vacancy called '$Z_{1/2}$ centre' has been identified as the primary lifetime-killing defect in the *n*-type SiC epitaxial layers and bulk material with density strongly dependent on the growth conditions [5–7].

Polarization of semi-insulating SiC is a common problem in the design of radiation detectors and other electronic components. The essence of the negative effect of polarization (space charge formation) is the deformation of the internal electric field [8,9,10,11,12]. The predisposition of semiconductor detectors to polarization is, according to our findings, highly influenced by the material quality that has been used in the detector fabrication (mainly the trap density and the substrate inhomogeneity). A previously published fact is that forming of

* Corresponding author.
E-mail address: praus@karlov.mff.cuni.cz (P. Praus).

https://doi.org/10.1016/j.rinp.2022.106110
Received 16 August 2022; Received in revised form 2 November 2022; Accepted 14 November 2022
Available online 15 November 2022

Ohmic metal electrical contacts influences chemical reactivity of 4H-SiC with most metals at elevated temperatures. Many metals react with SiC at relatively low temperatures to form silicides and carbon or carbides. The role of carbon in ohmic contact ranges from carbon precipitates, which are responsible for contact degradation, to carbon/graphite, which is a key factor for their ohmic properties. [13–16]. Over decades, the quality of the SiC epitaxial layers has enhanced. Schottky barrier diode (SBD) detectors produced on the epitaxial layers show no polarization effects [17,18,11,19] and their charge collection efficiency approaches 100 %. It was found that the charge collection properties are no longer affected by the defects due to the high quality of epitaxial 4H-SiC substrate [11].

Transport and spectroscopic properties of the bulk 4H-SiC detectors fabricated from the HPSI 4H-SiC wafers were investigated in detail during last decade [20,10,11]. The authors reported, that the bulk 4H-SiC detectors quickly polarized and the energy resolution was quite poor in contrast to the epitaxial SBD. The maximum CCE for bulk detectors reaches only 75 % [10] and 28 % [11] at bias −200 V and −500 V, respectively, just after bias application. From the fact that they obtained different values of the maximum CCE (even lower value for higher applied bias) we can deduce that the sufficient spectroscopic quality of the SiC wafers has not yet been reached.

Laser-induced transient current technique using DC or pulsed bias is widely used for the characterization of the charge transport and collection efficiency in radiation detectors, and for the determination of the kinetics of the detector polarization [21,12,22]. Applying pulsed bias, we are able to measure detector characteristics in the depolarized state [23,24,25,12,22]. The bias is periodically applied for a short time not sufficient for the space charge formation and then set to zero volts allowing temporarily formed space charge relaxation. Recently, Belas et. al. [26] used the pulse and DC biased L-TCT for the characterization of transport properties of the HPSI 4H–SiC bulk detectors equipped with gold electrodes. They had to overcome the problems with a very short electron lifetime observed in as-grown bulk samples, but also with frequency limitation and parasitic phenomena caused by the properties of the L-TCT electronic circuit. They actually observed current waveforms in the form of oscillations not sensitive to the applied bias, which completely overlapped the original current waveforms. They identified very short carrier lifetime ≤ 1 ns and the electric-field-induced damping of electron drift mobility. They also derived that the electron drift velocity saturates and the evaluated saturated value is 8.7×10^6 cm s^{-1}. They evaluated the defect level with the ionization energy of $E_D = 0.85$ eV and identified the wide impurity band below the Fermi level. The theoretical model developed in [26] is used and shortly described in this paper at the analysis of all experimental data. The principle of the model stems from an assumption of a saturated electron mobility at high bias and an existence of dispersed impurity level/band localized below Fermi energy, which is continuously charged due to electron depletion.

In this article, we investigate the effect of the metallization using metallic or graphene electrical contacts and the 4H-SiC wafer spatial homogeneity on the charge transport and spectroscopic properties of the bulk 4H-SiC sensors by the pulsed or DC biased L-TCT and alpha spectroscopy measurement. We also measure the time dependent variation of the space charge formation (detector polarization) using pulse biased L-TCT and present the long-term stable charge collection and energy resolution for alpha particles. The dynamic of the space charge formation is simulated by the theoretical model introduced in [26].

Experimental

We used undoped high purity semi-insulating (HPSI) 4H-SiC wafer produced by Cree Inc. with diameter $\varphi = 10$ cm, that was specified as an epitaxy-ready substrate (both sides were already polished). 4H-SiC material was *n*-type with the electrical conductivity $\sigma(300\ \mathrm{K}) = 3 \times 10^{-10}\ \Omega^{-1}\mathrm{cm}^{-1}$ dominated by a surface shunt. Free electron concentration $n(300\ \mathrm{K}) = 500\ \mathrm{cm}^{-3}$ was derived from the temperature dependent Hall effect measurement by an extrapolation of n(T) from the high-temperature data [26].

Wafer was cut to the chips with dimensions of 5 mm × 5 mm and thickness of 350 μm. Single sensors were prepared on the chips taken randomly from this set. We did not polish or etch sensors before (first) contact preparation. Sensors were only ultrasonically cleaned in toluene, acetone, methanol and isopropanol. We examined five types of sensor metallization using Au/Au, Ni/Ni, AuCr/CrAu, Cr/Cr (thermal evaporation) and graphene/graphene (G/G) semi-transparent electrical contacts. Graphene contacts were prepared by the thermal decomposition of SiC. The growth temperature was 1650 °C for 5 min in the pressure of 1 barr of Ar ambient. Ar pressure together with a 1 mm hole in a graphite crucible controls the partial pressure of silicon and the sublimation rate, as described in more detail in another paper of our group [27]. We verified the successful graphene layer growth by Raman spectroscopy.

We use our L–TCT experimental setup in pulsed or DC bias regimes to characterize SiC transport properties [25,12,26]. This setup is based on the high–frequency amplification of the current pulse passing on the AC coupled detector anode that is recorded by an ultrafast digital sampling oscilloscope. Due to the 4H-SiC energy band-gap $E_g = 3.26$ eV, we use above band-gap UV optical pulses (335 nm wavelength, ≈ 500 ps as FWHM and an illuminated spot of ∼ 1 mm^2) for generation of electron-hole pairs. UV pulses are generated as a second harmonic in the BBO crystal using the pulsed white continuum laser which is synchronously triggered by the master arbitrary waveform generator. Measuring conditions are characterized by four parameters; laser pulse delay (LPD), bias pulse width (BPW), depolarization time (DT) and laser pulse period (LPP). Pulsing parameters are kept the same for all sensors but they differ at respective measuring modes. The scheme of the L-TCT setup identical to [26] and detailed explanation of the L-TCT measurement conditions including time correlation of the optical and bias pulses are presented in the Supplement S1a.

Alpha spectra (^{241}Am) of the SiC sensors were recorded using a standard spectroscopic setup extended by the sensor depolarization functionality. Block scheme of the experimental setup is presented in Fig. 1(a). We are using in-house made charge sensitive preamplifier with the shortened recovery time (Gain = 50 mV/MeV, rise time ∼ 50 ns, $t_{recovery}$ ∼ 200 ms, Fall time ∼ 15.5 μs, noise FWHM 7 keV at 100 pF), shaping amplifier (Ortec 671) and MCA easy multi-channel analyzer (Ortec Easy 2 K). In order to eliminate the effect of the sensor polarization during alpha spectroscopy measurement we used pulsed bias and multi-channel analyzer (MCA) data acquisition synchronous gating. The gating was used to eliminate noise originating from bias switching. MCA gating with variable gate delay GD (relative to bias pulse) is also convenient for studying alpha spectra evolution. Timing of the bias pulse and MCA gate is shown in Fig. 1(b). During the first 250 ms the shaping amplifier is fully saturated by the bias step and cannot process any signal correctly. This region is highlighted in red in the timing diagram (Fig. 1b). Additional information on response characteristics of both amplifiers to the bias pulse can be found in the Supplement S1b. Alpha spectra are only acquired over the duration of the gate window throughout multiple bias pulses to obtain a sufficiently high number of counts. It is important to note that for studying alpha spectra shortly after biasing (250 ms-5 s) it is crucial to use a short gate window (GW = 50 ms-300 ms) as the samples are usually evolving quickly. Spectra evolution at later time (>5 s) can be studied in either pulsed or DC bias regime. However, acquisition time in a pulsed bias regime needs to be significantly longer due to prolonged depolarization time. We have found that DT at least twice the length of the bias pulse is sufficient for sample depolarization. In DC regime, the overall principle of measurement is the same, except that the collection window (30 s) is set by PC instead of MCA gate. However, we are still using GD to describe the relative position of the bias switch on and centre of the collection window.

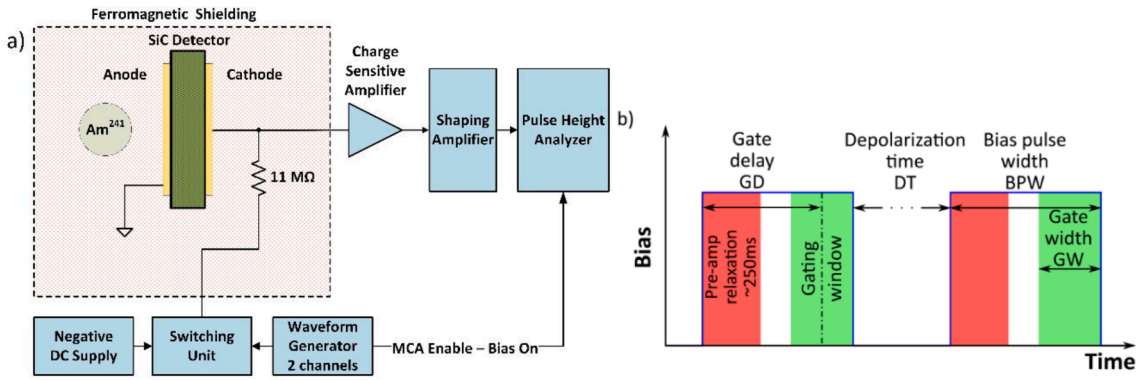

Fig. 1. (a) Alpha spectroscopy experimental setup. (b) The timing diagram of the bias pulsing and MCA gating. Bias pulsing period was set to 6 s with the detector depolarization time (DT) = 5.4 s. A delay time of 250 ms is set before the data collection begins. Data acquisition lasted 350 ms.

Results and discussion

Effect of metallization

First, we tested the effect of the metallization on the charge transport in the HPSI 4H-SiC bulk sensor prepared with Au/Au, Cr/Cr, Ni/Ni, AuCr/AuCr or graphene/graphene (G/G) electrodes. Metals have been chosen on the basis of scientific literature [13–16]. We selected one sensor cut from the wafer (sensor-T) and repeatedly deposited different metal contacts on the same sensor. Each metallization was polished off and then sensors were etched in hydrochloric acid before depositing a new type of contact. We believe this process had little to no effect on the surface layer (metal to metal substitution). Repeated preparation of Ni/Ni contacts on the same sensor led to almost the same current waveform shape and temporal evolution. In the case of graphene there may have been the same changes in the material due to the graphene growth process as is discussed later (Alpha spectroscopy of sensors). Using pulse biased L-TCT (see the Supplement S1a) we measured the sensor in an unpolarised state. We found that pulsing parameters BPW = 150 μs, LPD = 100 μs and DT = 100 ms are optimal to avoid space charge formation in all used sensors. BPW = 150 μs ensures that the space charge does not have enough time to form and DT = 100 ms allows its extinction (if any space charge had formed) before the next bias pulse. At these conditions, the sample's bulk may be assumed to be neutral immediately after

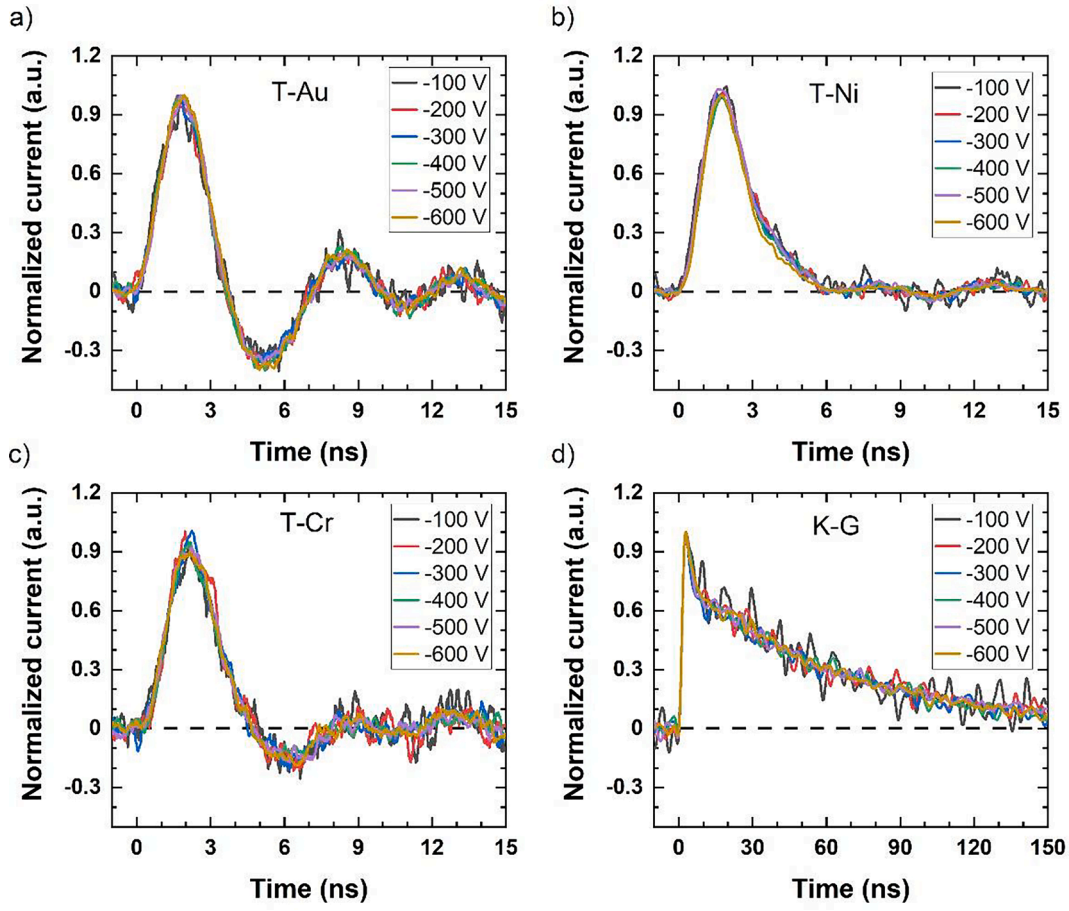

Fig. 2. Normalized pulsed L-TCT electron CWFs for sensor-T with (a) Au/Au, (b) Ni/Ni, c) Cr/Cr electrodes and d) for SiC-K with G/G electrodes.

biasing (LPD = 100 μs). Consequently, current waveforms (CWFs) obtained using these parameters are also stable long-term. In Fig. 2(a-c) we show normalized electron CWFs measured in the sensor-T with Au/Au, Cr/Cr, and Ni/Ni electrodes. The shape of the CWFs for the AuCr/CrAu contact was very similar to Au/Au. Therefore, we don't show the data here. Simultaneously we prepared another sensor (sensor-K) from a different part of the wafer, which was equipped with G/G contacts. CWFs for this sensor are presented in Fig. 2(d) for comparison.

Typical shape of current transient measured in good quality sensors with favourable mobility-lifetime product at pulse bias is characterized by a nearly constant weakly damped current transient. This shape represents the charge passage through the sensor, which is terminated by an abrupt damping when the charge reaches the collecting electrode (anode) [12]. In contrast to such behaviour, here in SiC we observed high-frequency attenuated oscillations for all metal electrodes identically with that observed in [26]. These oscillations with the period about 6 ns are caused by a RLC response of the electronic circuit to the fast rise and drop of the CWF. Significant component of damped harmonic oscillations was observed for Au/Au and AuCr/CrAu contacts and almost aperiodic waveforms are visible for Ni/Ni contacts. Nevertheless, the frequency of the oscillations is the bias independent for all metal contacts, while only amplitude increases with the bias. Observed oscillations are mostly affected by the short lifetime of charge carriers, the limited frequency bandwidth (3 GHz) of the amplifier and by parasitic inductances. These oscillations completely overlap the true CWFs and neither the drifting charge nor transit time representing the time when generated carriers reach opposite electrode can be determined [26]. We use complete sensor replacement circuit to determine the transfer function that has been used in theoretical simulation of CWFs using calculated values of single components. Detailed scheme and analysis of the replacement circuit is given in the Supplement S2.

The current transients of graphene-contacted sensor-K presented in Fig. 2(d) show significantly delayed non-oscillating CWFs with significantly extended afterglow about 100 ns comparing a few ns in case of sensors with metallic contacts. The fact that the unusual shape of CWFs appears selectively in the G/G sensor shows that the shape is directly related to the special design of the G/G sensor and the way of its preparation. We suggest following model explaining specified effects. The extended drift of photo-induced charge through the sensor is not caused by the charge propagation through the sensor but it is induced by a delayed collection of the signal in the graphene layer. As it was reported in [28,29], the graphene-semiconductor interface is a convenient host for surface plasmons localized on the graphene-semiconductor interface. We expect that plasmons may temporarily store the charge collected at the graphene cathode and slow-down the CWF detection. Obtained graphene waveform also has longer rise-time (compared to its metallic counterparts). We believe it is caused by different surface resistance and capacitance of the graphene contacts (more detailed discussion in the Supplement S2).

Based on obtained results we conclude that the damping and the oscillating shape of the electron CWFs is affected by specific conductivity of the contacts and the overall parasitic inductances.

Space charge formation in 4H-SiC sensors with metal contacts

Complementary to the analysis of the shape of CWFs affected by different metallization, we also investigated the space charge formation using the same sensor-T prepared with various electrical contacts. During this measurement, we use pulse and DC biased L-TCT, where CWFs were acquired at variable LPDs. It was found out that for LPD less than 100 ms fixed DT = 100 ms was sufficient for sample depolarization. For larger LPD, BPW scaled proportionally to LPD roughly as BPW ~ 1.1 LPD and DT = 2 BPW was used for depolarization. For LPD > 10 s, DC biasing was used with LPP = 10 ms. The scheme of pulsing conditions is presented in the Supplement S1a. We found out that the sensor-T polarizes similarly with any metallic contact manifesting the same progress after biasing. Fig. 3(a) shows the gradual evolution of the electron CWFs measured at DC bias −400 V for sensor-T with Au/Au electrical contacts. The amplitude of the oscillations rises for the initial 500 ms and then decreases for a long time. As we deduced in [26], the inactive region starts to form beneath the anode at this time. Further widening of the inactive region, i.e. the shortening of the depleted region, then leads to the decrease in collected charge. Simultaneously, the extrema of oscillations slightly shift to a shorter time, which was explained and confirmed by numerical simulations in [26] as a result of the shortened collection time in the detector with a significantly thinned depleted region in the polarized sensor. This behaviour is presented in more detail in Fig. 3(b), where we show time evolution of the collected charge of sensor-T with Au/Au, Ni/Ni and Cr/Cr contacts, respectively, for variable LPD using both pulsed or DC bias −400 V. The collected charge was calculated by integration of the CWFs over the first period of the oscillations. These dynamics of the space charge formation are independent on the sensor metallization.

Testing of the 4H-SiC wafer homogeneity

To explore wafer homogeneity, we used five sensors cut from different positions of the same 4H-SiC wafer. Three sensors labelled C, S and T were equipped with Au/Au electrodes and sensors E and K with AuCr/CrAu and G/G electrodes, respectively. The last two sensors were added for comparison, supposing space charge formation is independent on the type of metallization (see Fig. 3(b)). The collected charge dependence on variable LPD measured at pulsed and DC bias −400 V compared for sensors from different positions on the same wafer is shown in Fig. 4. Measuring conditions were the same as in the Section 3.2. The data for different sensors were normalized at initial time and then offset for better clarity. We can see that collected charge dependency has similar profile for each sensor, the only difference is the LPD position of the maximum of the collected charge. An evident shift of the maximum of the collected charge was found in sensors cut from different positions of the same wafer. According the Shockley-Read-Hall defect model [30,31], the rate of the space charge formation, which is closely tied to the position of the collected charge maximum, depends only on the concentration of defects, their position in the band gap and their capture cross-section. Results in Fig. 4 therefore suggest that either type and/or concentration of defects vary spatially in the studied sensors.

Theoretical curves in Fig. 4 were calculated based on the model overviewed in the Supplement S3, we are also presented model parameters. Using this model, we calculated the space charge density that reached rather high value in the 14th order. Respective values are shown for measured sensors in Table 1. This is a pretty large charge density for the radiation detectors and is in agreement with unsatisfactory sensor characteristics.

We also tested electric current relaxation measurement in sensors step-biased by DC bias as a simple method of the characterization of sensor polarization. This method could be a less experimentally demanding procedure instead of L-TCT. The temporal evolution of the electric current of various sensors (same as in Fig. 4) after step-biasing to the DC bias 400 V is presented in Fig. 5.

We may see that most of samples revealed characteristic profiles composed of a weak initial drop followed by steady current enhancement. We assign the drop by an initial exhaustion of electron traps, which supply electrons to a depleted sensor shortly after the biasing. Subsequent current increase is then affected by the electron supply at the cathode due to an amplified electric field in this region. Most of samples (T, S, K, and C) show the minimum at the time similar to the position of maximum in CCE in Fig. 4. However, we have to note here, that the measurement of the electric current relaxation is not a general method for the characterization of the sensor polarization. We can see that for the slowly polarizing sensor E current does not pass the minimum in Fig. 5. The same effect is assumed for a sensor with very fast polarization

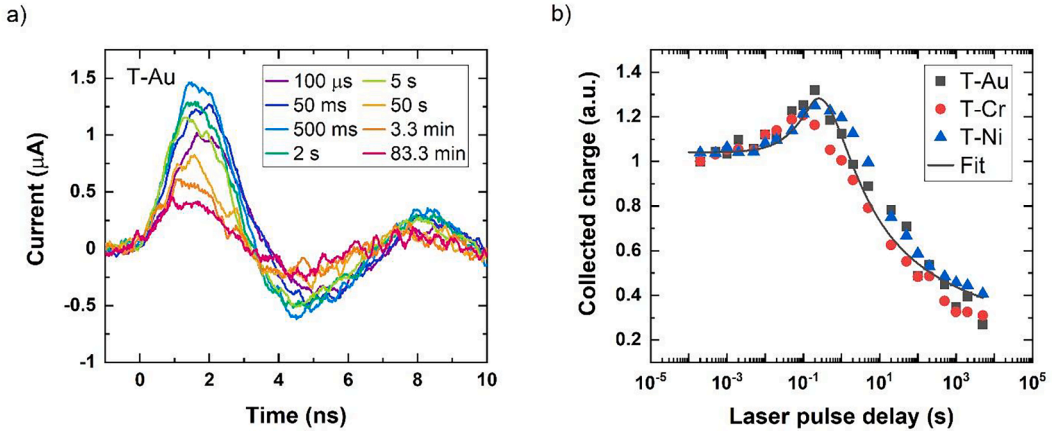

Fig. 3. (a) Time degradation of the electron CWFs for Au/Au sensor-T at DC bias −400 V. (b) The collected charge dependence on variable LPD using pulsed and DC bias −400 V of sensor-T with Au/Au, Ni/Ni and Cr/Cr contacts, respectively. The black solid line represents fitted dependence according to the theoretical model [26].

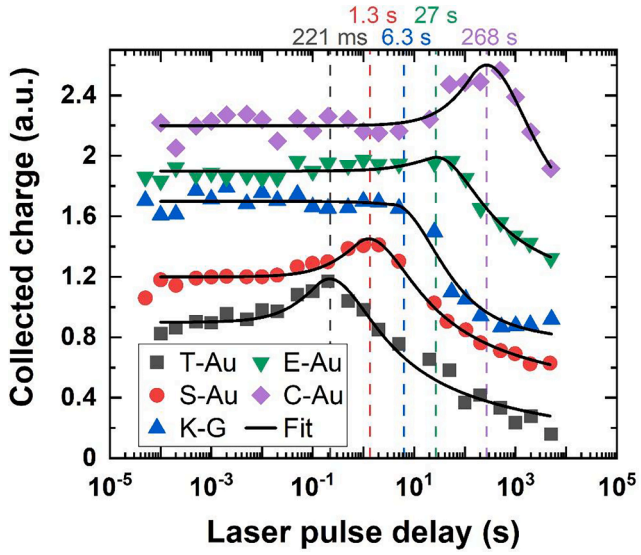

Fig. 4. Collected charge dependence on variable laser pulse delay compared for different sensor chips with the same Au/Au metallization. Additional sensors with G/G and AuCr/CrAu contacts are given for the comparison. Black solid lines represent fits according to the theoretical model (in colour). The CCE of each sensor is normalized to unity at the initial time and shifted gradually with the step 0.3 for the better resolution.

Table 1
Space charge density in respective sensors biased at 400 V and 10^4 s.

Sensor	T (Au, Cr, Ni)	S (Au)	C (Au, Cr)	E (CrAu)	K (G)
Space charge density at 10^4 s (cm^{-3})	1.7×10^{14}	1.8×10^{14}	3.7×10^{14}	6.1×10^{14}	7.0×10^{14}

at the time of less than 1 s.

Based on the obtained results we conclude that the different metallization has only a minor effect on the dynamics of the space charge formation of the sensor. The principal reason of unlike behaviour of respective sensors is their variable defect structure, i.e. an inhomogeneity corresponding to different position of the sensor on the wafer. Discovered correspondence between the time evolution of collected charge and the rate of the space charge formation allows finding places in the wafer with slow polarization using L-TCT.

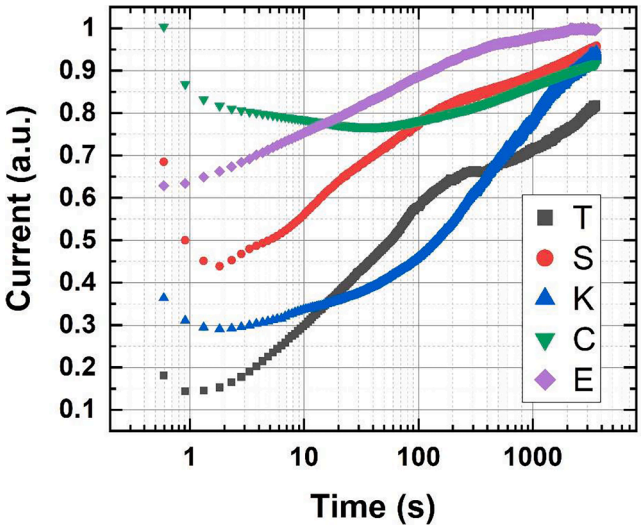

Fig. 5. Temporal evolution of electric current in investigated sensors biased at 400 V.

Alpha spectroscopy of sensors

We tested sensor response for alpha particle radiation using the ^{241}Am alpha source for all five sensors mentioned in Section 3.3. In Fig. 6 we show strong time-degradation of the alpha spectra for sensor-S with Au/Au contacts at DC bias −400 V. The respective temporal evolution of the charge collection efficiency (CCE) measured at pulsed (up to GD = 10 s) and DC (GD > 10 s) bias −400 V using our alpha spectroscopy setup with depolarization functionality is shown in Fig. 7 for SiC sensors cut from the different wafer positions, each prepared with Au/Au electrodes. Sensors E and K with AuCr/CrAu and G/G electrodes, respectively, were again added for the comparison. Comparing Fig. 4 and Fig. 7, we see good agreement in the position of maxima at CCE in all cases. Consistently with the results presented in Fig. 4, we observe the onset of CCE initially and subsequent decrease in the efficiency of the charge collection in all sensors. On the other hand, the peak shape in Fig. 6 seems to narrow with decreasing charge collection. This is, however, only the smearing of the spectra due to the fast CCE evolution in the beginning (collection window 30 s). As the space charge formation slows down collected spectra become symmetric and their FWHM also decreases.

Maximal theoretical collected charge (MCA channel) was

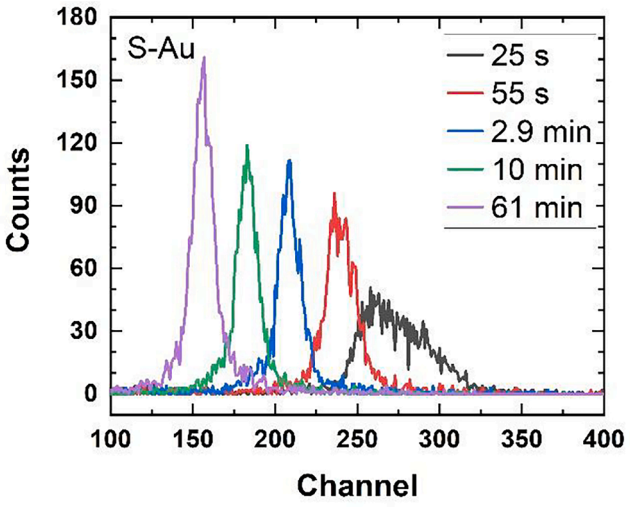

Fig. 6. Time dependence of the alpha spectra shape for the sensor-S with Au/Au contacts for −400 V DC bias. Alpha spectra were collected over 30 s wide gating window (see experimental).

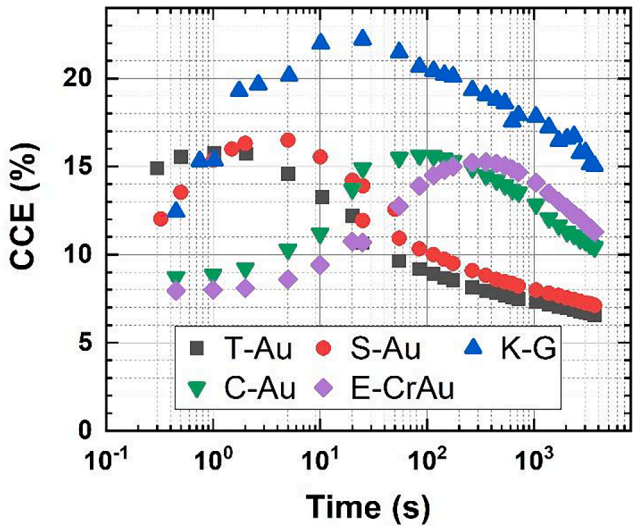

Fig. 7. Time dependence of the Charge collection efficiency of alpha radiation in different sensors defined in the text biased at −400 V.

determined using CdTe detector and recalculated to SiC using their electron-hole pair creation energies $E_{e\text{-}h}$(CdTe) = 4.50 eV and E_{eh}(SiC) = 7.28 eV [32,33]. We found that the used pulsed bias with pulse detection gating leads to long-term stabilization of the charge collection for all types of metallization as well as sensors. This makes it possible to successfully use such an inhomogeneous SiC wafer to fabricate an alpha detection sensor.

Particular attention should be paid to the sensor equipped with graphene contacts due to their different behaviour and possible unique properties [35–39]. Although the basic features of results obtained on this sensor are similar to the sensors with metal contacts, we may identify significant deviations. They may be characterized by following results: (i) The time evolution of collected charge behaves differently when measured by L-TCT and alpha spectroscopy. In the case of L-TCT it does not pass through the maximum detected at sensors with metal contacts, see Fig. 4. (ii) The alpha spectrum evolves unusually, splitting to the low energy and high energy peaks, see Fig. 8. The collected charge is, however increased, see Fig. 7. (iii) After changing the graphene contact to the chromium one, the CWF shape transformed to the

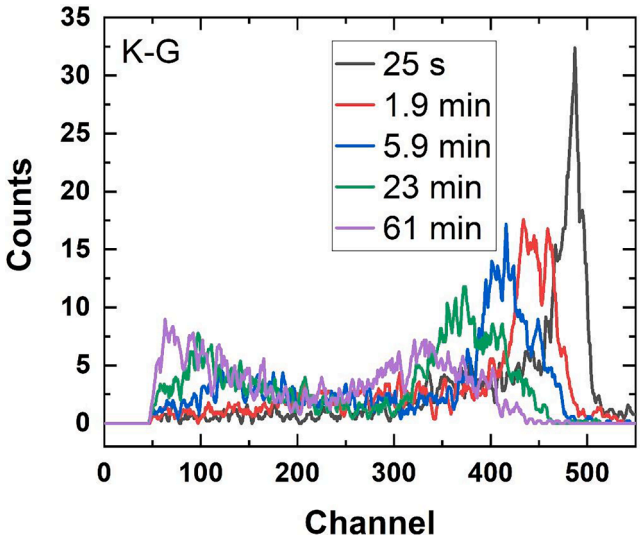

Fig. 8. Time dependence of the alpha spectra shape for the sensor-K with G/G contacts for −400 V DC bias.

oscillatory-type shape analogous to Cr/Cr contacted originally, see Fig. 2 (c). The splitting of the alpha-spectra and enhanced CCE further outlasted. Not shown in this paper.

Items (i)-(iii) probably relate to the method of the sensor's preparation involving the heating to 1650 °C for 5 min. This process probably led to a change of the subsurface layer inducing an abundant formation of micro pipe defects hourly reported in the literature [34]. Simultaneously, a severe inhomogeneity of the defect structure and of electric properties could appear there. Item (i) may be then explained by different depth profiles of photo-excited carriers induced by the laser light and alpha radiation in SiC [37,11]. Assuming that the light absorbs more likely closer to the surface, where the electric field could be partly screened by additional charged defects and the lifetime of electrons could be further lowered, the expected maximum in CCE could be suppressed as it is seen in Fig. 4. In contrast to the surface damage, the electron lifetime in the sensor's bulk is enhanced by the annealing, that is represented by the CCE accentuation, Fig. 7. The enhancement of carrier lifetime in annealed SiC was reported in [7]. (ii) Splitting of the alpha spectrum points to principal lateral inhomogeneity of the sensor showing two characteristic regions. These regions are distributed randomly through the whole sensor's plane since the spectra splitting was observed in different spots of the sensor. We suggest micro pipe defects are responsible for this feature. When the alpha particle is captured in the unperturbed region of the sensor, the collected charge is large and a contribution to the high-energy peak is accounted. Oppositely, the capturing near micro pipe results in the low CCE mediated by enhanced trapping in that region. The effect cannot be observed at L-TCT, which covers the macroscopic area and microscopic features at the surface cannot be distinguished. Item (iii) proves our concept confirming that the shape of CWFs is connected with the type of contact while (i) and (ii) are induced by the treatment at the sample's preparation.

Finally, we conclude that the electron CWFs shape is affected by specific conductivity of the contacts and the overall parasitic inductances. In contrast, different metallization has only a minor effect on the dynamics of the space charge formation of all sensors. The polarization rate of the individual sensors is influenced by the wafer spatial inhomogeneity of the defect structure.

Summary

We investigated transport properties of HPSI 4H-SiC bulk sensors equipped with different types of electrodes and the effect of spatial inhomogeneity on the space charge formation in the prepared sensors

using L-TCT and alpha spectroscopy. We found that SiC sensors polarize quickly after applying DC bias. By application of pulsed bias with the depolarization time DT $>$ 100 ms, we were able to fully depolarize the detector and achieve long-term stable charge collection for any used contact and sensor. The shape of the L-TCT current waveforms in the depolarized sensors depends on the specific conductivity of the used electrodes and parasitic inductances. In the case of a sensor with graphene contacts, the shape of CWFs differs significantly, due to the lower graphene conductivity and a formation of subsurface damage layer caused by sample heating during the graphene formation. The dynamics of space charge formation in all sensors is insensitive to the used electrodes, but strongly depends on the sensor's original position on the wafer, suggesting spatial inhomogeneity of the used wafer. We observed continuous space charge formation leading to CCE evolution with the local maximum appearing 0.2 s-270 s after biasing for different sensors. The space charge formation was successfully depicted by the presented theoretical model, which allowed us to simulate the space charge formation and fit the charge collection efficiency data. The space charge density exceeding 10^{14} cm^{-3} after long term biasing was obtained in all samples. Similar dynamics of the polarization was deduced from the electric current relaxation measurement, where the position of the current minimum reflects CCE maxima. Careful analysis of current relaxations can be used as an experimentally less demanding alternative to L-TCT. Finally, we can say that using the L-TCT method we are able to find places in the wafer with slow polarization and prepare sensors with long-term stable charge collection efficiency.

Charge collection evolution studied by ^{241}Am alpha spectroscopy further affirms the results obtained by L-TCT and current relaxation analysis. We found that CCE ranges from 5 % (fastest polarizing samples) to 24 % (at CCE maximum of G/G sensor). The unusual behaviour of the G/G sample represented by the splitting of the spectrum was attributed to the graphene preparation method, which may have affected the sensor's structure.

CRediT authorship contribution statement

P. Praus: Writing – original draft, Writing – review & editing, Conceptualization, Methodology. **M. Betušiak:** Data curation, Formal analysis. **E. Belas:** Supervision, Conceptualization, Writing – original draft. **J. Kunc:** Methodology, Validation. **R. Grill:** Formal analysis, Investigation, Writing – original draft. **M. Brynza:** Data curation. **J. Pipek:** Software, Data curation.

Declaration of Competing Interest

The authors declare that they have no known competing financial interests or personal relationships that could have appeared to influence the work reported in this paper.

Data availability

Data will be made available on request.

Acknowledgements

This work was financially supported by the Czech Science Foundation under project No. P102/18-12449S and by the Charles University Grant Agency under contract No. GAUK 379621.

Appendix A. Supplementary data

Supplementary data to this article can be found online at https://doi.org/10.1016/j.rinp.2022.106110.

References

[1] Mohapatra S, Abhangi M, Vala S, Sahu PK, Rath S, Narasimha Murty NVL. Comparative study of Single Crystal (SC)-Diamond and 4H-SiC bulk radiation detectors for room temperature alpha spectroscopy. J Instrum 2021;16:06020.
[2] Kleppinger JW, Chaudhuri SK, Karadavut O, Nag R, Watson DLP, McGregor DS, et al. Deep-level transient spectroscopy and radiation detection performance studies on neutron irradiated 250-μm-thick 4H-SiC epitaxial layers. IEEE Trans Nucl Sci 2022;69(8):1972–8.
[3] Bertuccio G, Casiraghi R. Study of Silicon Carbide for X-Ray Detection and Spectroscopy. IEEE Trans Nucl Sci 2003;50(1):175–85.
[4] Nava F, Bertuccio G, Cavallini A, Vittone E. Silicon carbide and its use as a radiation detector material. Meas Sci Technol 2008;19:102001.
[5] Klein PB, Shanabrook BV, Huh SW, Polyakov AY, Skowronski M. Lifetime-limiting defects in 4H-SiC epilayers. Appl Phys Lett 2006;88:052110.
[6] Kimoto T, Niwa H, Okuda T, Saito E, Zhao Y, Asada S, et al. Carrier lifetime and breakdown phenomena in SiC power device material. J Phys D Appl Phys 2018;51:363001.
[7] Jenny JR, Malta DP, Tsvetkov VF, Das MK, Hobgood H, Mc D, et al. Effects of annealing on carrier lifetime in 4H-SiC. J Appl Phys 2006;100:113710.
[8] Kleppinger JW, Chaudhuri SK, Karadavut O, Mandal KC. Defect characterization and charge transport measurements in high-resolution Ni/n-4H-SiC Schottky barrier radiation detectors fabricated on 250 um epitaxial layers. J Appl Phys 2021;129:244501.
[9] Puglisi D, Bertuccio G. Silicon Carbide Microstrip Radiation Detectors. Micromachines 2019;10(12):835.
[10] Bertuccio G, Puglisi D, Pullia A, Lanzieri C. X- gamma Ray Spectroscopy With Semi-Insulating 4H-Silicon Carbide. IEEE Trans Nucl Sci 2013;60(2):1436–41.
[11] Raja PV, Akhtar J, Rao CVS, Vala R, Abhangi M, Murty NVL. Spectroscopic performance studies of 4H-SiC detectors for fusion alpha-particle diagnostics. Nucl Instrum Methods in Phys ResA 2017;869:118–27.
[12] Belas E, Grill R, Pipek J, Praus P, Bok J, Musiienko A, et al. Space charge formation in chromium compensated GaAs radiation detectors. J Phys D Appl Phys 2020;53:475102.
[13] Wang Z, Liu W, Wang Ch. Recent Progress in Ohmic Contacts to Silicon Carbide for High-Temperature Applications. J Electronic Materials 2016;45(1):267–84.
[14] Nikitina IP, Vassilewski KV, Wright NG, Horsfall AB, O'Neil AG. Formation and role of graphite and nickel silicide in nickel based ohmic contacts to n-type silicon carbide. J Appl Phys 2005;97:83709.
[15] Cheng Y, Lu W, Wang T, Chen Z. Fabrication of Ohmic contact on semi-insulating 4H-SiC substrate by laser thermal annealing. J Appl Phys 2016;119:225705.
[16] Lu W, Mitchel WC, Landis GR, Crenshaw TR, Collins WE. Catalytic graphitization and Ohmic contact formation on 4H–SiC. J Appl Phys 2003;93:5397.
[17] Bertuccio G, Caccia S, Puglisi D, Macera D. Advances in Silicon Carbide X-ray Detectors. Nucl Instr Meth A 2011;652:193–6.
[18] Mandal KC, Muzykov PG, Terry JR. Highly sensitive x-ray detectors in the low energy range on n-type 4H-SiC epitaxial layers. Appl Phys Lett 2012;101:051111.
[19] Mandal K, Kleppinger JW, Chaudhuri SK. Advances in High-Resolution Radiation Detection Using 4H-SiC Epitaxial Layer Devices. Micromachines 2020;11:254.
[20] Mandal KC, Krishna RM, Muzykov PG, Das S, Sudarshan TS. Characterization of Semi-Insulating 4H Silicon Carbide for Radiation Detectors. IEEE Trans Nucl Sci 2011;58(4):1992–9.
[21] Musiienko A, Grill R, Pekárek J, Belas E, Praus P, Pipek J, Dědič V, Elhadidy H. Characterization of polarizing semiconductor radiation detectors by laser-induced transient currents. Appl Phys Lett 2017;111:082103.
[22] Musiienko A, Pipek J, Praus P, Brynza M, Belas E, Dryzhakov B, et al. Deciphering the effect of traps on electronic charge transport properties of methylammonium lead tribromide perovskite. Sci Adv 2020;6:eabb6393.
[23] Suzuki K, Sawada T, Imai K. Effect of DC Bias Field on the Time-of-Flight Current Waveforms of CdTe and CdZnTe Detectors. IEEE Trans Nucl Sci 2011;58(4):1958.
[24] Cola A, Farella I, Anni M, Martucci MC. Charge Transients by Variable Wavelength Optical Pulses in CdTe Nuclear Detectors. IEEE Trans Nucl Sci 2012;59(4):1569.
[25] Praus P, Belas E, Bok J, Grill R, Pekárek J. Laser Induced Transient Current Pulse Shape Formation in (CdZn)Te Detectors. IEEE Trans Nucl Sci 2016;63(1):246.
[26] Belas E, Betušiak M, Grill R, Praus P, Brynza M, Pipek J, et al. Space charge formation in the high purity semi-insulating bulk 4H–silicon carbide. J Alloy Compd 2022;904:164078.
[27] Kunc J, Rejhon M, Belas E, Dědič V, Moravec P, Franc J. Effect of Residual Gas Composition on Epitaxial Growth of Graphene on SiC. Phys Rev Applied 2017;8:04401131.
[28] Principi A, Vignale G, Carrega M, Polini M. Intrinsic lifetime of Dirac plasmons in graphene. Phys Rev B 2013;88:195405.
[29] Kumada N, Dubourget R, Sasaki K, Tanabe S, Hibino H, Kamata H, et al. Plasmon transport and its guiding in graphene. New J Phys 2014;16:063055.
[30] Shockley W, Read WT. Statistics of the Recombinations of Holes and Electrons. Phys Rev 1952;87:835.
[31] Look DC. The electrical characterization of semi-insulating GaAs: A correlation with mass-spectrographic analysis. J Appl Phys 1977;48:5141.
[32] Takahashi T, Watanabe S, Kouda M, Sato G, Okada Y, Kubo S, et al. High-resolution CdTe detector and applications to imaging devices. IEEE Trans Nucl Sci 2001;48(3):287–91.
[33] Chaudhuri SK, Zavalla KJ, Mandal KC. Experimental determination of electron-hole pair creation energy in 4H-SiC epitaxial layer: An absolute calibration approach. Appl Phys Lett 2013;102:031109.
[34] Neudeck PG, Powell JA. Performance Limiting Micropipe Defects in Silicon Carbide Wafers, *IEEE Electron*. Dev Lett 1994;15(2):63.

[35] Shobhit K, Patel SK, Surve J, Parmar J. Detection of cancer with graphene metasurface-based highly efficient sensors. Diam Relat Mater 2022;129:109367.
[36] El-Ahmar S, Przychodnia M, Jankowski J, Prokopowicz R, Ziemba M, Szary MJ, et al. The Comparison of InSb-Based Thin Films and Graphene on SiC for Magnetic Diagnostics under Extreme Conditions. Sensors 2022;14:5258.
[37] Sridhara SG, Devaty RP, Choyke WJ. Absorption coefficient of 4H silicon carbide from 3900 to 3250 Å. J Appl Phys 1998;84:2963–4.
[38] Kunc J, Rejhon M, Belas E, Dědič V, Moravec P, Franc J. Effect of Residual Gas Composition on Epitaxial Growth of Graphene on SiC. Phys Rev Applied 2017;8:044011.
[39] Uxa S, Belas E, Grill R, Praus P, James RB. Determination of Electric Field Profile in CdTe and CdZnTe Detectors Using Transient-Current Technique. IEEE Trans Nucl Sci 2012;59:2402.